iScience, Volume *24*

Supplemental Information

Brd2/4 and Myc regulate alternative cell lineage programmes during early osteoclast differentiation in vitro

Valentina S. Caputo, Nikolaos Trasanidis, Xiaolin Xiao, Mark E. Robinson, Alexia Katsarou, Kanagaraju Ponnusamy, Rab K. Prinjha, Nicholas Smithers, Aristeidis Chaidos, Holger W. Auner, and Anastasios Karadimitris

Supplementary File

Brd2/4 and Myc regulate alternative cell lineage programmes during early osteoclast development in vitro

Valentina S Caputo[1]*, Nikolaos Trasanidis[1]*, Xiaolin Xiao[1]*, Mark E Robinson[1], Alexia Katsarou[1,2], Kanagaraju Ponnusamy[1], Rab K Prinjha[3], Nicholas Smithers[3], Aristeidis Chaidos[1,2], Holger W Auner[1,2] and Anastasios Karadimitris[1,2†]

[1]Hugh & Josseline Langmuir Centre for Myeloma Research, Centre for Haematology, Department of Immunology and Inflammation, Imperial College London, London, UK
[2]Department of Haematology, Hammersmith Hospital, Imperial College Healthcare NHS Foundation Trust, London, UK
[3]Medicines Research Centre, GlaxoSmithKline, Stevenage, United Kingdom

Transparent methods

Cell culture

RAW264.7 cells were maintained in DMEM media (Sigma) containing 10% FBS (Life technologies), 1000U/ml penicillin/streptomycin (Sigma). HEK293T cells were cultured in DMEM media (Sigma) supplemented with 10% FBS (Sigma). Cells were grown at 37^0C under 5% CO2.

Primary osteoclast and Osteoclast progenitors

Bone marrow cells (BM) were harvested from murine tibias and femurs of C57BL/6 male mice, washed with PBS. Red cells were lysed with RCL (eBioscience) and washed again with PBS. To obtain osteoclast progenitors (OCP), BM cells were stained with anti-CD11b PerCP, -CD3e FITC, -CD115 PE, -B220 FITC and -cKIT APC (from BD Pharmingen) using standard protocols and flow-sorted as described in (Hu et al., 2011) using a BD FACSAriaII flow-sorter.

BM cells were cultured in α-MEM (Life technologies) containing 10% FBS (Life technologies) and 1% penicillin-streptomycin (Sigma) and 20 ng/ml M-CSF (Preprotech) overnight at a density of 1×10^6 cells/ml. Non-adherent BM cells were harvested the next day as source of primary osteoclasts.

Osteoclast assays

Osteoclast progenitors (OCP) and non-adherent BM cells were seeded into 24/48 or 96 well/plates in complete media with 20 ng/ml M-CSF (Preprotech) and 50 ng/ml RANKL (Preprotech) at a density of 1×10^6 cells/ml (1ml per 24 w, 500ul /48w and 200 ul/ 96 well). RAW264.7 cell were seeded at a density of 1×10^6 cells/ml (1ml per 24 w, 500ul /48w and 200 ul/ 96 well) and cultured in presence of 50ng/ml RANKL (Preprotec)

For all the cultures, after 2-3 days of culture, media was changed. After 6-7 dyas the cells were fixed and stained for TRAP activity using the TRAP assay kit (Sigma).

Multinucleated cells with 3 or more nuclei were counted as TRAP+ cells. Images were acquired using EVOS cell imagine system (Thermofisher) (Ersek et al., 2015).

shRNA constructs and lentivirus production

ShRNA oligoes were phosphorylated and annealed and cloned, using the AgeI and EcoRI sites into a modified lentiviral pLKO.1 vector (Sigma), in which the puromycin gene had been replaced with eGFP. A scrambled shRNA was used as control. The following oligoes were used for the shRNA cloning:

-*Sh Mm MYC Forward primer*: 5'-
CCGGGACTCCGTACAGCCCTATTTCCTCGAGGAAATAGGGCTGTACGGAGTCTTTTTG-3'
-*Sh Mm MYC Reverse primer*: 5'-
AATTCAAAAAGACTCCGTACAGCCCTATTTCCTCGAGGAAATAGGGCTGTACGGAGTC
-3'

Recombinant lentiviruses were produced by co-transfecting the pLKO.1-GFPshRNA plasmid with helper plasmids (pRSV.REV, pMDLgpRRE and pMD2.VSVG) into HEK293T cells using the calcium phosphate method. After 24h of transfection, the medium was replaced. Viral supernatant was collected at 48h and 72h post transfection. Lentiviruses were concentrated by ultracentrifugation at 23000rpm for 1.5h at 4^0C. Cells were transduced in the presence of polybrene (8µg/ml final concentration; Sigma). Two days post-transduction, GFP positive cells were FACS-sorted using a BD FACSAriaII flow-sorter.

Reverse transcription PCR and qRT-PCR

Total RNA was isolated from cultured cells using the ReliaPrep RNA cell Miniprep System (Promega). cDNA was synthesized with RevertAid cDNA synthesis kit (Thermoscientific). qRT-PCR was performed with Taqman probes (Applied Biosystems) using an AB StepOne Plus Real-Time PCR (Applied Biosystems). Gene expression was normalized to the expression of *HPRT* housekeeping gene using the ΔCt method. Taqman probes: *Myc* (Mm00487804_m1), *Brd2* (Mm01271171_s1), *Brd4* (Mm00480394_m1), *Nfatc1* (Mm00479445_m1), *Irf8* (Mm00492567_m1), *Ocstamp* (Mm00512445_m1), *Dcstam*p (Mm04209236_m1) and *Hprt* (Mm00446968_m1).

RNA-seq

Total RNA was isolated from RAW264.7 cells at 0, 4, 14 and 24h after RANKL, RANKL/I-BET, I-BET- treatment (two independent experiments per time point and condition) using the Nucleospin RNA kit (Macherey-Nagel). RNA quantity was determined with Qubit using the Qubit RNA Assay kit (Life Technologies) and RNA quality was assessed on the Bioanalyser using the RNA pico kit (Agilent). Libraries were prepared using the NEBNext poly(A) mRNA Magnetic Isolation Module and the NEBNext Ultra RNA Library Prep kit for Illumina (NEB), following manufacturer's instructions. Library quantity was determined using the Qubit High Sensitivity DNA kit (Life Technologies) and library size was determined using the Bioanalyser High Sensitivity DNA kit (Agilent). Libraries were quantified using the Universal Library Quantification Kit for Illumina (Kapa Biosystems) and run on AB StepOne Plus Real-Time PCR (Applied Biosystems). Libraries were diluted to 2nM and sequenced using the Illumina HiSeq 2500 platform to obtain paired-end 100bp reads. Two replicate per time point and treatment were made.

Chromatin immunoprecipitation

Chromatin immunoprecipitation (ChIP)-qPCR was performed as described in (Caputo et al., 2013). Specifically, after 4 h treatment RAW264.7 cells were washed with PBS and crosslinked with 1% formaldehyde (SIGMA) for 15 min at room temperature.

Crosslinking was stopped by the addition of glycine (1.25M) to a final 125 mM concentration. Subsequently, the cells were washed 3 times with ice cold PBS and pelleted at 300g. The crosslinked cells were lysed for 20 min on ice, and the nuclei were sonicated for 5 times for 5 min each time using a 30sec/30 sec off cycles, at 4^0C, under high intensity in a Bioruptor UCD-200 (Diagenode).
Sonicated fragments ranged 500-300bp in length. The sonicated chromatin was diluted at least ten times with ChIP dilution buffer (0,01%SDS, 1,1% Triton X-100, 1,2mM EDTA, 16,7mM Tris-HCL pH 8, 167mM NaCl) with freshly added proteinase inhibitors (Sigma). To avoid unspecific binding, the diluted chromatin was pre-cleared for 1h at 4^0 C with magnetic beads (Dynabeads Protein A+G form Invitrogen). 3-5ug of antibody was added to pre-cleared chromatin aliquots and incubated overnight at 4^0C on a rotating wheel.
Immunoprecipitation was achieved by addition of protein A+G (50% each) magnetic beads and incubating for 2-4h at 4^0C on a rotating wheel. Immunoprecipitated complexes were washed for 5 min with salt buffer (0.1% SDS, 1% Triton X-100, 2mM EDTA, 20mM Tris-HCl pH 8, 150mM NaCl), high salt buffer (0.1% SDS, 1% Triton X-100, 2mM EDTA, 20mM Tris-HCl pH 8, 500mM NaCl), LiCl buffer (0,25M LiCl, 1 % IGEPAL, 1% sodium deoxicolate, 1mM EDTA, 10mM Tris-HCl pH 8) and TE. All the washed were perform twice at 4^0C on a rotating wheel.
Elution and un-crosslinking were achieved by incubating the immoprecipitated complexes with 150μl elution buffer (50mM Tris-HCl pH 8, 50mM NaCl, 1mM EDTA and freshly added 1% SDS and 20mg/ml of RNaseA) at 65^0C overnight and again a second time for 30 min. Eluted complexes were treated with proteinase K (Thermoscientific) for 45 min at 45^0C.
DNA was purified by phenol extraction and ethanol DNA precipitation. Q-PCR was performed using SYBR Select Master Mix (Lifetechnologies) on a StepOne Plus Real-Time PCR (Applied Biosystems). Enrichment of the target sequence was assessed against INP DNA and IgG control (C1111), cMYC (sc764), Max (SC197), Brd2 (Bethyl A302-582A). Brd3 (Bethyl A302-368A) and Brd4 (Bethyl A301-985150), H3K27ac (ab4729).

ChIP-seq
Treated and untreated cells were cultured using DMEM medium.10^7 cells per ChIP were cross-linked with 1% formaldehyde for 15min. Chromatin immunoprecipitation was performed as described above. The ChIP DNA was purified with AMPure beads (Beckman). ChIP and input DNA libraries were prepared using the NEBNext ChIP-seq Library Prep Master Mix for Illumina (NEB) following manufacturer's protocols. The quantity was determined using the Qubit High Sensitivity DNA kit (Life Technologies) and library size was determined using the Bioanalyser High Sensitivity DNA kit (Agilent). Libraries concentration was quantified using the Universal Library Quantification Kit for Illumina (Kapa Biosystems) using a AB StepOne Plus Real-Time PCR (Applied Biosystems). Libraries were diluted to a final concentration of 2nM and sequenced at the MRC Imperial facility using the Illumina HiSeq 2500 platform to obtain single-end 50bp reads.

ATAC-seq
ATAC seq was performed as described in (Buenrostro et al., 2015). Briefly, 50.000 cells were collected and washed at 500g at 4^0C for 5 min with PBS. The cell pellet was resuspended in ATAC lysis buffer and immediately spun for 10 min at 500g at 4^0C. The nuclei were then subjected to Tn reaction for 30 min at 37^0C; the reaction was terminated and the DNA purified immediately using a MinElute Kit (Qiagen). The purified DNA was amplified with NEBNext High-Fidelity 2x PCR Master Mix (NEB). The PCR amplified product was cleaned with AMPure beads (Beckman). The quality of the libraries was assessed with the Bioanalyser High Sensitivity DNA kit (Agilent). The library was quantified with using the Universal Library Quantification Kit for

Illumina (Kapa Biosystems) on a StepOne Plus Real-Time PCR (Applied Biosystems). The libraries were sequenced at the Genomics Facility at MRC/LIMS of ICL using the Illumina HiSeq 2500 platform to obtain paired-end 100bp reads.

Bioinformatic analysis

ChIP-Seq

ChIP-Seq normalisation and analysis

Bowtie 2.3.4.1 (64 bit) was used to map ChIP-Seq reads to the mm10 mouse reference genome using default parameters and samtools 1.2 was used to convert SAM files, sorting and indexing BAM files. The Picard package was used to remove duplicated reads and the reads mapped on unknown and random chromosomes, in BAM files. MACS2 (v2.1) was used for peaks calling for each sample (Brd, Myc, Max, and H3K27ac) against their corresponding control input DNA. Significant peaks were obtained by applying an appropriate q-value cutoff (Brds, broad peaks calling at q<0.05; Myc, narrow peaks calling at q<0.1; Max, narrow peaks calling at q<0.01; H3K27ac, broad peaks calling at q<0.01). The significant ChIP-Seq peaks from MACS2 were annotated using the ChIPpeakAnno (Zhu, 2013; Zhu et al., 2010) and Homer package against the built-in mm10 mouse genome with the default settings. The R/Bioconductor package Diffbind (Ross-Innes et al., 2012) was used to obtain differential binding sites (DBS) across different conditions (R, RI, I, S) for samples (Brd and H3K27ac). For this purpose, three pseudo-replicates per ChIPseq sample were obtained by down-sampling to the minimum read depth; only peaks detected consistently in 2 out of 3 pseudo-replicates were used for DBS analysis. Furthermore, bedops tools were used on Brd2 and Brd4 DBS to generate Venn diagrams (**Figure 2E**) for different comparisons. The ChIPpeakAnno package was also used to annotate all significant DBS (FDR<0.05) and identify overlaps between H3K27ac annotated regions with the Brds significant DBS (FDR<0.05).

In addition, the Homer tools *findMotifsGenome* function was used to perform known and de-novo motifs analysis against the built-in mm10 mouse genome for the significant ChIP-Seq peaks (Figure 4E).

Super-enhancer calling

To identify the list of super-enhancers (SE) for each condition (S,R,RI,I), the significantly enriched H3K27ac peaks obtained from MACS2 were analysed further using the Ranking Of Super Enhancers (ROSE) package (Whyte et al., 2013) (Loven et al., 2013) (**Figure 3D**). Correspondingly, the SE regions were annotated using the ChIPpeakAnno package

Genomic regions visualization

The IGV Genome Browser was used for genomic regions visualization. The DeepTools toolkit (Ramirez et al., 2016) was used to generate heatmaps and metagene plots of the Brd2,3,4 signal over the significant DBS(FDR<0.05: -10kb - +10kb region around the peak center) (Figure 2D), and the choromatin analysis and exploration (ChAsE) (Younesy et al., 2016) tool was applied to visualize Input, Myc and Max ChIPseq signals (±2 kb around the peak center) (Figure 4C).

RNA-Seq

The pair-end reads from the RNA-Seq experiments for all the 4 conditions (S/R/Ri/I) across the different time points (0, 4, 14 and 24h) were aligned to the GRCm38 (mm10) reference genome by STAR (version 2.5.3a) with 10,000 as the max number of different alignments per read to consider (--alignTranscriptsPerReadNmax 100000). To ensure the large reads files to be processed smoothly, the limits settings in STAR were increased (--limitGenomeGenerateRAM 20000000000). The “Rsubread” (version 1.24.2) R/Bioconductor package was used to obtain the raw read counts per

library using the GRCm38 reference genome. The "DESeq2" (version 1.16.1) (Love et al., 2014) R/Bioconductor package was used for normalising the counts and implementing the Differential Gene Expression (DGE) analysis across timepoints and treatments. The R package "pheatmap" was used to draw the initial clustered heatmaps for the selected differential expressed genes (|lfc|>0.8 and padj<0.05) of each contrast across conditions. The correlation was computed as the dissimilarity between the selected DEGs in order to capture their expression changes across all the time points (h0, h4, h14 and h24). Then an R package for performing Weighted Gene Co-expression Network Analysis (WGCNA) (Langfelder and Horvath, 2008) (Zhang and Horvath, 2005) was used to find clusters (modules) of highly correlated genes based on the dendrogram tree of the initial clustered heatmaps. Comparative PCA and MA plots were generated using the PCA and maPlot functions in R. Gene set enrichment analysis (enriched GO, pathways, etc.) was performed for the clusters using enrichR (Chen et al., 2013; Kuleshov et al., 2016)

ATAC-Seq

ATAC-Seq reads were trimmed using TrimGallore (--paired -q 30 --nextera) and aligned against the mm10 mouse reference genome using Bowtie 2.3.4.1(-X 2000). SAM files conversion and BAM files sorting and indexing were performed using samtools. The picard and samtools packages were used to remove duplicate reads and reads mapped on chrUn, chr_random and chrM chromosomes, respectively. Peak calling was performed using MACS2 (*-B –nomodel –call-summits -q 0.01*) and deepTools functions were used to obtain pileup tracks. The ENCODE backlisted regions for mm10 were removed using bedtools (https://www.nature.com/articles/s41598-019-45839-z). The pyDNAse (Wellington) algorithm was used for TF footprinting; the genome-wide Tn5 cut site tracks (bigwig), the Tn5 signal per TF and the predicted TF biding sites were obtained using the default package parameters. TF motif calling on significant footprints (cutoff=20) was performed using Homer against HOCOMOCOv11 core database. To remove redundant and overlapping motifs, motif similarity was determined using TomTom from the MEME suite, and grouped into highly similar motif-classes (q<0.01). To predict the most likely candidate TF responsible for each footprint, all TF within the motif-class detected in the footprint region were ranked by an overall score of expression level and change in osteoclastogenesis ($-\log_{10}(padj)*|\log_2FC|*\log_2(RPKM+1)$), and highest scoring TF selected. Only TF genes were considered for GRN visualization, as plotted with the igraph package.

Integrative Analysis

Integrative analysis on ChIPseq and RNAseq data

The Beta package (Binding and Expression Target Analysis) was applied to integrate the Myc ChIP-Seq data with Differential Expressed (DE) genes from RNA-Seq data across different time points (4, 14, and 24 h). Also, ChIP-Seq data (Brd, and H3K27ac) and their differential binding sites (Brd DBS and H3K27ac DBS) were annotated to the closest differentially expressed gene.

Published datasets usage

The previously published RNA-Seq data (SRP096890) and Irf8/Pu.1 ChIPseq were used for additional comparisons and validation (Langlais et al., 2016).

Data availability

All data are accessible from Gene Expression Omnibus database (Acc. Number: GSE160840).

Supplementary Figure Legends

Figure S1, Related to Figure 1. Transcriptional and cellular responses of RAW264.7 and primary precursor cells to RANKL and I-BET151. (**A**) Flow cytometry strategy for identification and isolation of osteoclast progenitors. (**B**) Top: TRAP staining of RAW264.7, bone-marrow OC precursors (BM OCP) and purified osteoclast progenitors upon treatment with RANKL (50ng/ml) and RANKL/I-BET151 (500nM); n=2-6 independent experiments in triplicates. Bottom: quantification of TRAP+ cells/well per condition. Results represent mean and SEM t test; ***, p=0.0001; ****, p< 0.0001 (**C**) Correlation matrix comparing overlap between significantly up- and down- regulated genes identified in RAW264.7 cells 24h post RANKL-induction with those of primary OC at 48h (WT Myc R vs S, (Bae et al., 2017)). Color key represents corresponding odds ratios. (**D**) Time course qPCR profiling of *Myc, Irf8, Dcstamp and Ocstamp* expression in murine primary bone marrow-derived pre-osteoclast cells; (n=3 mice). Results represent mean and SEM (One-way ANOVA: **, p<0.01; ***, p<0.001; ****, p<0.0001). (**E**) RNA-seq analysis in RAW264.7 cells. Top: PCA analysis of differentially expressed genes (12 clusters derived from R vs S analysis) across time points (4,14,24hr) and comparisons (RvsS, IvsS, RvsI and RvsRI); bottom: MA plot of 12 gene clusters across comparisons at 24h after treatments.

Figure S2. Related to Figure 1. Dynamic transcriptional alterations during early osteoclast development in response to RANKL and I-BET151. (A) Time course profiling of *Nfatc1* expression after RANKL-, I-BET151- or RANKL/I-BET151 treatment (left, qRT-PCR; right, RNAseq); values were normalized to time 0. (**B**) Enrichment analysis (left: ChEA, right: Mouse Gene Atlas) on 156 genes included in Cluster 7 (displayed in **Fig1B**). (**C**) Heatmap illustration of pairwise treatment comparisons (R vs S, I vs. S, RI vs R) at 0,4,14 and 24h, as analysed by RNA-Seq in RAW 264.7 cells. **(D)** qPCR profiling of *Myc, Irf8, Dcstamp and Ocstamp* expression in murine primary bone marrow-derived pre-osteoclast cells 4h after no treatment (S), treatment with RANKL (R), RANKL/I-BET151 (RI) or I-BET151; (n=3 mice). Results represent mean and SEM (One-way ANOVA: *, p<0.05; **, p<0.01)

Figure S3, related to Figure 2. Time course profiling of BET proteins expression after RANKL-, IBET151- or RANKL/I-BET151 treatments. (**A**) RNA-Seq and (**B**) qRT-PCR time course experiments.

Figure S4, related to Figure 3. Functional annotation of transcriptional responses associated with Brd2,4 chromatin binding. (**A**) Line plots indicating expression patters of all predicted target genes with increased associated Brd2,4 binding in RANKL treated cells. (**B**) IGV snapshot illustrating the Brd4 and H3K27ac enrichment, along with the identified super-enhancer, across S,R,I conditions on the *Fos* genetic locus. Overrepresentation analysis of differentially expressed genes at 4 (**C**) and 14h (**D**) associated with super-enhancer (SE) and typical enhancer (E) regulation**.** EnrichR analysis using databases: ChEA, KEGG pathways, Gene ontology, WIKI pathways and NCI nature.

Figure S5, **related to Figure 4. The gene regulatory network of the early developmental events during osteoclast development.** (**A**) Genome-wide Tn5

footprinting profiles for each transcription factor. (**B**) Time course profiling of *Myc* expression at 0, 4, 14 and 24h after RANKL, I-BET151 or RANKL/I-BET151 treatment using qRT-PCR and RNA-seq (**C**). Individual regulatory modules for indicated TF. Arrow width indicates footprint score for originating TF at target gene promoter/enhancer, colour indicates direction of expression change for originating TF. Node size indicates strength of expression change ($-\log_{10}(padj)*|\log_2 FC|$) and colour indicates direction of change at 14h post-RANKL treatment, (Red=upregulated and blue=downregulated).

Figure S6, **related to Figure 4. Phenotypic and epigenomic characterization of *Myc* at the early stages of osteoclast development.** *Myc* mRNA, TRAP OC assay and TRAP+ OC numbers/well after treatment shRNA-mediated *Myc* knock-down (shMyc) in RAW 274.7 cells (**A**) or (**B**) their treatment with the Myc-Max inhibitor 10058-F4 (F4 50mM). *Myc* expression is shown relative to *Hprt* and scrbl or un-treated cells, respectively; n=3-5 independent experiments with triplicate technical replicates. (**C**) The epigenomic landscape of the 560 Myc-bound regions in developing osteoclasts. Violin plots displaying the relative enrichment ($\log_2$ scale) of H3K27ac and Brd2-4 on the Myc-bound regions across S, R, RI and I conditions. (**D)** EnrichR overrepresentation analysis of differentially expressed genes (14h post RANKL-induction) with associated Myc and Brd2,4 binding sites. EnrichR analysis (ChEA, KEGG pathways, Gene ontology, WIKI pathways and NCI nature). *, $p<0.05$; ***, $p<0.001$; ****, $p<0.0001$.

References

Azuma, Y., Kaji, K., Katogi, R., Takeshita, S., and Kudo, A. (2000). Tumor necrosis factor-alpha induces differentiation of and bone resorption by osteoclasts. J Biol Chem *275*, 4858-4864.

Bae, S., Lee, M. J., Mun, S. H., Giannopoulou, E. G., Yong-Gonzalez, V., Cross, J. R., Murata, K., Giguere, V., van der Meulen, M., and Park-Min, K. H. (2017). MYC-dependent oxidative metabolism regulates osteoclastogenesis via nuclear receptor ERRalpha. J Clin Invest *127*, 2555-2568.

Baud'huin, M., Lamoureux, F., Jacques, C., Rodriguez Calleja, L., Quillard, T., Charrier, C., Amiaud, J., Berreur, M., Brounais-LeRoyer, B., Owen, R.*, et al.* (2017). Inhibition of BET proteins and epigenetic signaling as a potential treatment for osteoporosis. Bone *94*, 10-21.

Boyce, B. F. (2013). Advances in the regulation of osteoclasts and osteoclast functions. J Dent Res *92*, 860-867.

Buenrostro, J. D., Wu, B., Chang, H. Y., and Greenleaf, W. J. (2015). ATAC-seq: A Method for Assaying Chromatin Accessibility Genome-Wide. Curr Protoc Mol Biol *109*, 21 29 21-21 29 29.

Caputo, V. S., Costa, J. R., Makarona, K., Georgiou, E., Layton, D. M., Roberts, I., and Karadimitris, A. (2013). Mechanism of Polycomb recruitment to CpG islands revealed by inherited disease-associated mutation. Hum Mol Genet *22*, 3187-3194.

Carey, H. A., Hildreth, B. E., 3rd, Geisler, J. A., Nickel, M. C., Cabrera, J., Ghosh, S., Jiang, Y., Yan, J., Lee, J., Makam, S.*, et al.* (2018). Enhancer variants reveal a conserved transcription factor network governed by PU.1 during osteoclast differentiation. Bone Res *6*, 8.

Charles, J. F., and Aliprantis, A. O. (2014). Osteoclasts: more than 'bone eaters'. Trends Mol Med *20*, 449-459.

Chen, E. Y., Tan, C. M., Kou, Y., Duan, Q., Wang, Z., Meirelles, G. V., Clark, N. R., and Ma'ayan, A. (2013). Enrichr: interactive and collaborative HTML5 gene list enrichment analysis tool. BMC Bioinformatics *14*, 128.

Chiang, C. M. (2009). Brd4 engagement from chromatin targeting to transcriptional regulation: selective contact with acetylated histone H3 and H4. F1000 Biol Rep *1*, 98.

Collin-Osdoby, P., and Osdoby, P. (2012). RANKL-mediated osteoclast formation from murine RAW 264.7 cells. Methods Mol Biol *816*, 187-202.

Collin-Osdoby, P., Yu, X., Zheng, H., and Osdoby, P. (2003). RANKL-mediated osteoclast formation from murine RAW 264.7 cells. Methods Mol Med *80*, 153-166.
Davidson, R. K., Himes, E. R., Takigawa, S., Chen, A., Horn, M. R., Meijome, T., Wallace, J. M., Kacena, M. A., Yokota, H., Nguyen, A. V., and Li, J. (2020). The loss of STAT3 in mature osteoclasts has detrimental effects on bone structure. PLoS One *15*, e0236891.

Edwards, C. M., Zhuang, J., and Mundy, G. R. (2008). The pathogenesis of the bone disease of multiple myeloma. Bone *42*, 1007-1013.

Ersek, A., Xu, K., Antonopoulos, A., Butters, T. D., Santo, A. E., Vattakuzhi, Y., Williams, L. M., Goudevenou, K., Danks, L., Freidin, A.*, et al.* (2015). Glycosphingolipid synthesis inhibition limits osteoclast activation and myeloma bone disease. J Clin Invest *125*, 2279-2292.

Fernandez-Alonso, R., Davidson, L., Hukelmann, J., Zengerle, M., Prescott, A. R., Lamond, A., Ciulli, A., Sapkota, G. P., and Findlay, G. M. (2017). Brd4-Brd2 isoform switching coordinates pluripotent exit and Smad2-dependent lineage specification. EMBO Rep *18*, 1108-1122.

Franzoso, G., Carlson, L., Xing, L., Poljak, L., Shores, E. W., Brown, K. D., Leonardi, A., Tran, T., Boyce, B. F., and Siebenlist, U. (1997). Requirement for NF-kappaB in osteoclast and B-cell development. Genes Dev *11*, 3482-3496.

Hnisz, D., Abraham, B. J., Lee, T. I., Lau, A., Saint-Andre, V., Sigova, A. A., Hoke, H. A., and Young, R. A. (2013). Super-enhancers in the control of cell identity and disease. Cell *155*, 934-947.

Hsu, H., Lacey, D. L., Dunstan, C. R., Solovyev, I., Colombero, A., Timms, E., Tan, H. L., Elliott, G., Kelley, M. J., Sarosi, I.*, et al.* (1999). Tumor necrosis factor receptor family member RANK mediates osteoclast differentiation and activation induced by osteoprotegerin ligand. Proc Natl Acad Sci U S A *96*, 3540-3545.

Hu, M., Bassett, J. H., Danks, L., Howell, P. G., Xu, K., Spanoudakis, E., Kotsianidis, I., Boyde, A., Williams, G. R., Horwood, N.*, et al.* (2011). Activated invariant NKT cells regulate osteoclast development and function. J Immunol *186*, 2910-2917.

Huijbregts, L., Petersen, M. B. K., Berthault, C., Hansson, M., Aiello, V., Rachdi, L., Grapin-Botton, A., Honore, C., and Scharfmann, R. (2019). Bromodomain and Extra Terminal Protein Inhibitors Promote Pancreatic Endocrine Cell Fate. Diabetes *68*, 761-773.

Izawa, N., Kurotaki, D., Nomura, S., Fujita, T., Omata, Y., Yasui, T., Hirose, J., Matsumoto, T., Saito, T., Kadono, Y.*, et al.* (2019). Cooperation of PU.1 With IRF8 and NFATc1 Defines Chromatin Landscapes During RANKL-Induced Osteoclastogenesis. J Bone Miner Res *34*, 1143-1154.

Kim, K., Kim, J. H., Lee, J., Jin, H. M., Kook, H., Kim, K. K., Lee, S. Y., and Kim, N. (2007). MafB negatively regulates RANKL-mediated osteoclast differentiation. Blood *109*, 3253-3259.

Kukita, T., Wada, N., Kukita, A., Kakimoto, T., Sandra, F., Toh, K., Nagata, K., Iijima, T., Horiuchi, M., Matsusaki, H.*, et al.* (2004). RANKL-induced DC-STAMP is essential for osteoclastogenesis. J Exp Med *200*, 941-946.

Kuleshov, M. V., Jones, M. R., Rouillard, A. D., Fernandez, N. F., Duan, Q., Wang, Z., Koplev, S., Jenkins, S. L., Jagodnik, K. M., Lachmann, A.*, et al.* (2016). Enrichr: a comprehensive gene set enrichment analysis web server 2016 update. Nucleic Acids Res *44*, W90-97.

Kurotaki, D., Yoshida, H., and Tamura, T. (2020). Epigenetic and transcriptional regulation of osteoclast differentiation. Bone *138*, 115471.

Lamoureux, F., Baud'huin, M., Rodriguez Calleja, L., Jacques, C., Berreur, M., Redini, F., Lecanda, F., Bradner, J. E., Heymann, D., and Ory, B. (2014). Selective inhibition of BET bromodomain epigenetic signalling interferes with the bone-associated tumour vicious cycle. Nat Commun *5*, 3511.

Langfelder, P., and Horvath, S. (2008). WGCNA: an R package for weighted correlation network analysis. BMC Bioinformatics *9*, 559.

Langlais, D., Barreiro, L. B., and Gros, P. (2016). The macrophage IRF8/IRF1 regulome is required for protection against infections and is associated with chronic inflammation. J Exp Med *213*, 585-603.

Le Pape, F., Vargas, G., and Clezardin, P. (2016). The role of osteoclasts in breast cancer bone metastasis. J Bone Oncol *5*, 93-95.

Lee, J. E., Park, Y. K., Park, S., Jang, Y., Waring, N., Dey, A., Ozato, K., Lai, B., Peng, W., and Ge, K. (2017). Brd4 binds to active enhancers to control cell identity gene induction in adipogenesis and myogenesis. Nat Commun *8*, 2217.

LeRoy, G., Rickards, B., and Flint, S. J. (2008). The double bromodomain proteins Brd2 and Brd3 couple histone acetylation to transcription. Mol Cell *30*, 51-60.

Love, M. I., Huber, W., and Anders, S. (2014). Moderated estimation of fold change and dispersion for RNA-seq data with DESeq2. Genome Biol *15*, 550.

Loven, J., Hoke, H. A., Lin, C. Y., Lau, A., Orlando, D. A., Vakoc, C. R., Bradner, J. E., Lee, T. I., and Young, R. A. (2013). Selective inhibition of tumor oncogenes by disruption of super-enhancers. Cell *153*, 320-334.

Miyauchi, Y., Ninomiya, K., Miyamoto, H., Sakamoto, A., Iwasaki, R., Hoshi, H., Miyamoto, K., Hao, W., Yoshida, S., Morioka, H.*, et al.* (2010). The Blimp1-Bcl6 axis is critical to regulate osteoclast differentiation and bone homeostasis. J Exp Med *207*, 751-762.

Nishikawa, K., Nakashima, T., Hayashi, M., Fukunaga, T., Kato, S., Kodama, T., Takahashi, S., Calame, K., and Takayanagi, H. (2010). Blimp1-mediated repression of negative regulators is required for osteoclast differentiation. Proc Natl Acad Sci U S A *107*, 3117-3122.

Park-Min, K. H., Lim, E., Lee, M. J., Park, S. H., Giannopoulou, E., Yarilina, A., van der Meulen, M., Zhao, B., Smithers, N., Witherington, J.*, et al.* (2014). Inhibition of osteoclastogenesis and inflammatory bone resorption by targeting BET proteins and epigenetic regulation. Nat Commun *5*, 5418.

Rahman, S., Sowa, M. E., Ottinger, M., Smith, J. A., Shi, Y., Harper, J. W., and Howley, P. M. (2011). The Brd4 extraterminal domain confers transcription activation independent of pTEFb by recruiting multiple proteins, including NSD3. Mol Cell Biol *31*, 2641-2652.

Ramirez, F., Ryan, D. P., Gruning, B., Bhardwaj, V., Kilpert, F., Richter, A. S., Heyne, S., Dundar, F., and Manke, T. (2016). deepTools2: a next generation web server for deep-sequencing data analysis. Nucleic Acids Res *44*, W160-165.

Raschke, W. C., Baird, S., Ralph, P., and Nakoinz, I. (1978). Functional macrophage cell lines transformed by Abelson leukemia virus. Cell *15*, 261-267.

Roe, J. S., Mercan, F., Rivera, K., Pappin, D. J., and Vakoc, C. R. (2015). BET Bromodomain Inhibition Suppresses the Function of Hematopoietic Transcription Factors in Acute Myeloid Leukemia. Mol Cell *58*, 1028-1039.

Ross-Innes, C. S., Stark, R., Teschendorff, A. E., Holmes, K. A., Ali, H. R., Dunning, M. J., Brown, G. D., Gojis, O., Ellis, I. O., Green, A. R.*, et al.* (2012). Differential oestrogen receptor binding is associated with clinical outcome in breast cancer. Nature *481*, 389-393.

Soysa, N. S., Alles, N., Aoki, K., and Ohya, K. (2012). Osteoclast formation and differentiation: an overview. J Med Dent Sci *59*, 65-74.

Sundaram, K., Nishimura, R., Senn, J., Youssef, R. F., London, S. D., and Reddy, S. V. (2007). RANK ligand signaling modulates the matrix metalloproteinase-9 gene expression during osteoclast differentiation. Exp Cell Res *313*, 168-178.

Takayanagi, H., Kim, S., Koga, T., Nishina, H., Isshiki, M., Yoshida, H., Saiura, A., Isobe, M., Yokochi, T., Inoue, J.*, et al.* (2002). Induction and activation of the transcription factor NFATc1 (NFAT2) integrate RANKL signaling in terminal differentiation of osteoclasts. Dev Cell *3*, 889-901.

Teitelbaum, S. L. (2000). Bone resorption by osteoclasts. Science *289*, 1504-1508.
Troen, B. R. (2006). The regulation of cathepsin K gene expression. Ann N Y Acad Sci *1068*, 165-172.

Wagner, E. F. (2002). Functions of AP1 (Fos/Jun) in bone development. Ann Rheum Dis *61 Suppl 2*, ii40-42.

Whyte, W. A., Orlando, D. A., Hnisz, D., Abraham, B. J., Lin, C. Y., Kagey, M. H., Rahl, P. B., Lee, T. I., and Young, R. A. (2013). Master transcription factors and mediator establish super-enhancers at key cell identity genes. Cell *153*, 307-319.

Wu, H., Xu, G., and Li, Y. P. (2009). Atp6v0d2 is an essential component of the osteoclast-specific proton pump that mediates extracellular acidification in bone resorption. J Bone Miner Res *24*, 871-885.

Yang, M., Birnbaum, M. J., MacKay, C. A., Mason-Savas, A., Thompson, B., and Odgren, P. R. (2008). Osteoclast stimulatory transmembrane protein (OC-STAMP), a novel protein induced by RANKL that promotes osteoclast differentiation. J Cell Physiol *215*, 497-505.

Younesy, H., Nielsen, C. B., Lorincz, M. C., Jones, S. J., Karimi, M. M., and Moller, T. (2016). ChAsE: chromatin analysis and exploration tool. Bioinformatics *32*, 3324-3326.

Yu, C., Niu, X., Jin, F., Liu, Z., Jin, C., and Lai, L. (2016). Structure-based Inhibitor Design for the Intrinsically Disordered Protein c-Myc. Sci Rep *6*, 22298.

Zhang, B., and Horvath, S. (2005). A general framework for weighted gene co-expression network analysis. Stat Appl Genet Mol Biol *4*, Article17.

Zhao, B., Takami, M., Yamada, A., Wang, X., Koga, T., Hu, X., Tamura, T., Ozato, K., Choi, Y., Ivashkiv, L. B.*, et al.* (2009). Interferon regulatory factor-8 regulates bone metabolism by suppressing osteoclastogenesis. Nat Med *15*, 1066-1071.

Zhu, L. J. (2013). Integrative analysis of ChIP-chip and ChIP-seq dataset. Methods Mol Biol *1067*, 105-124.

Zhu, L. J., Gazin, C., Lawson, N. D., Pages, H., Lin, S. M., Lapointe, D. S., and Green, M. R. (2010). ChIPpeakAnno: a Bioconductor package to annotate ChIP-seq and ChIP-chip data. BMC Bioinformatics *11*, 237.

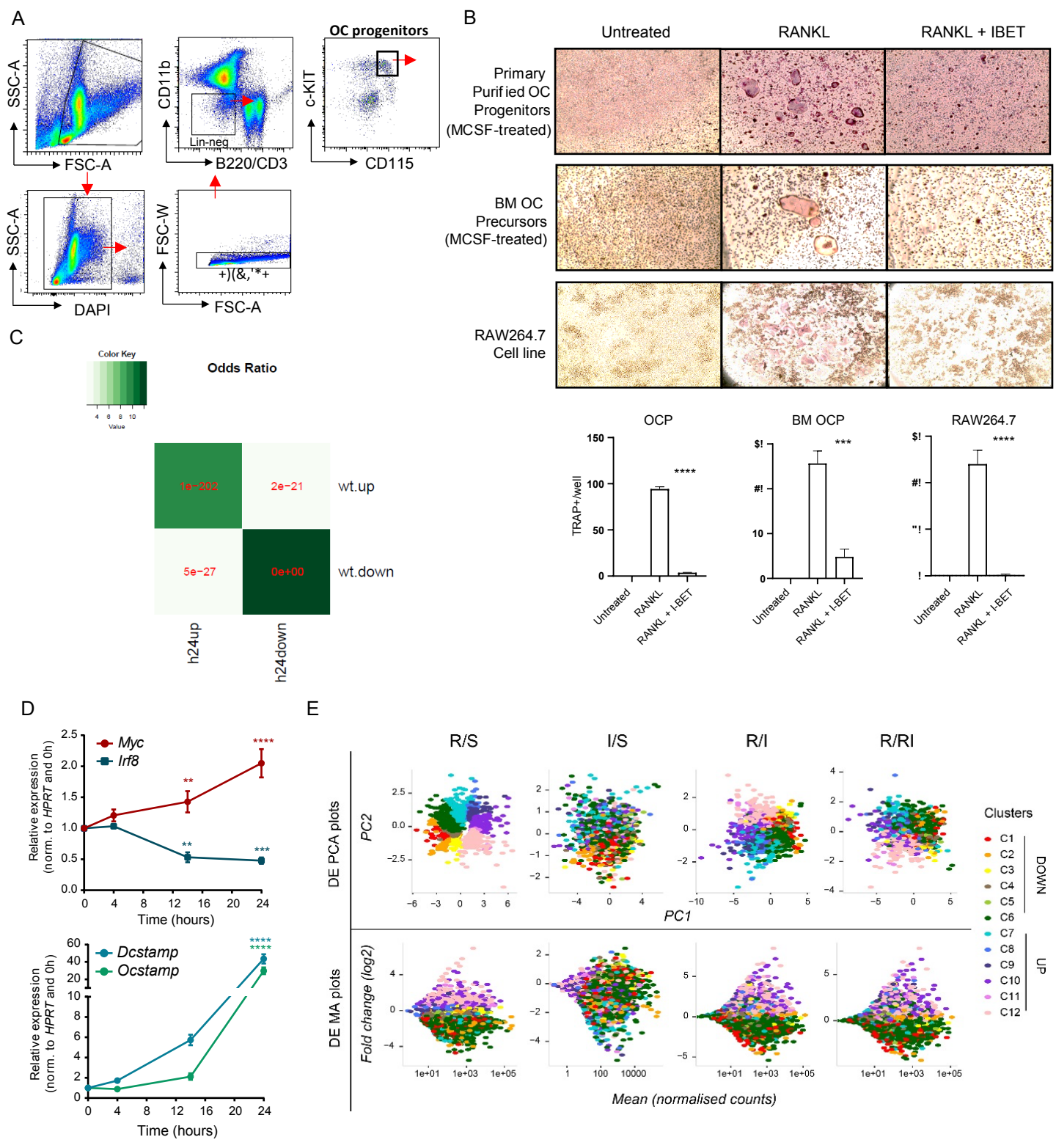

Suppl Figure 1

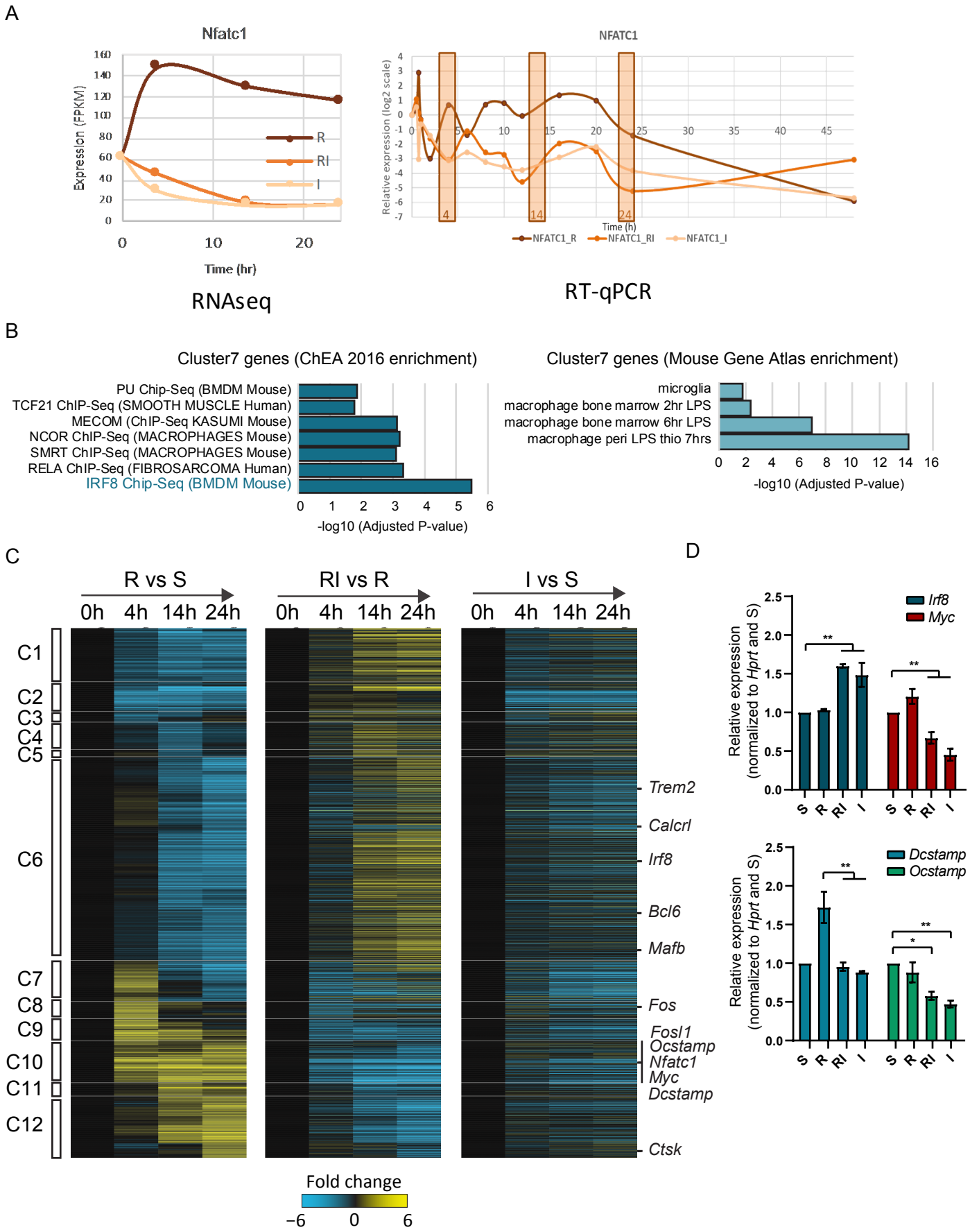

Suppl. Figure 2

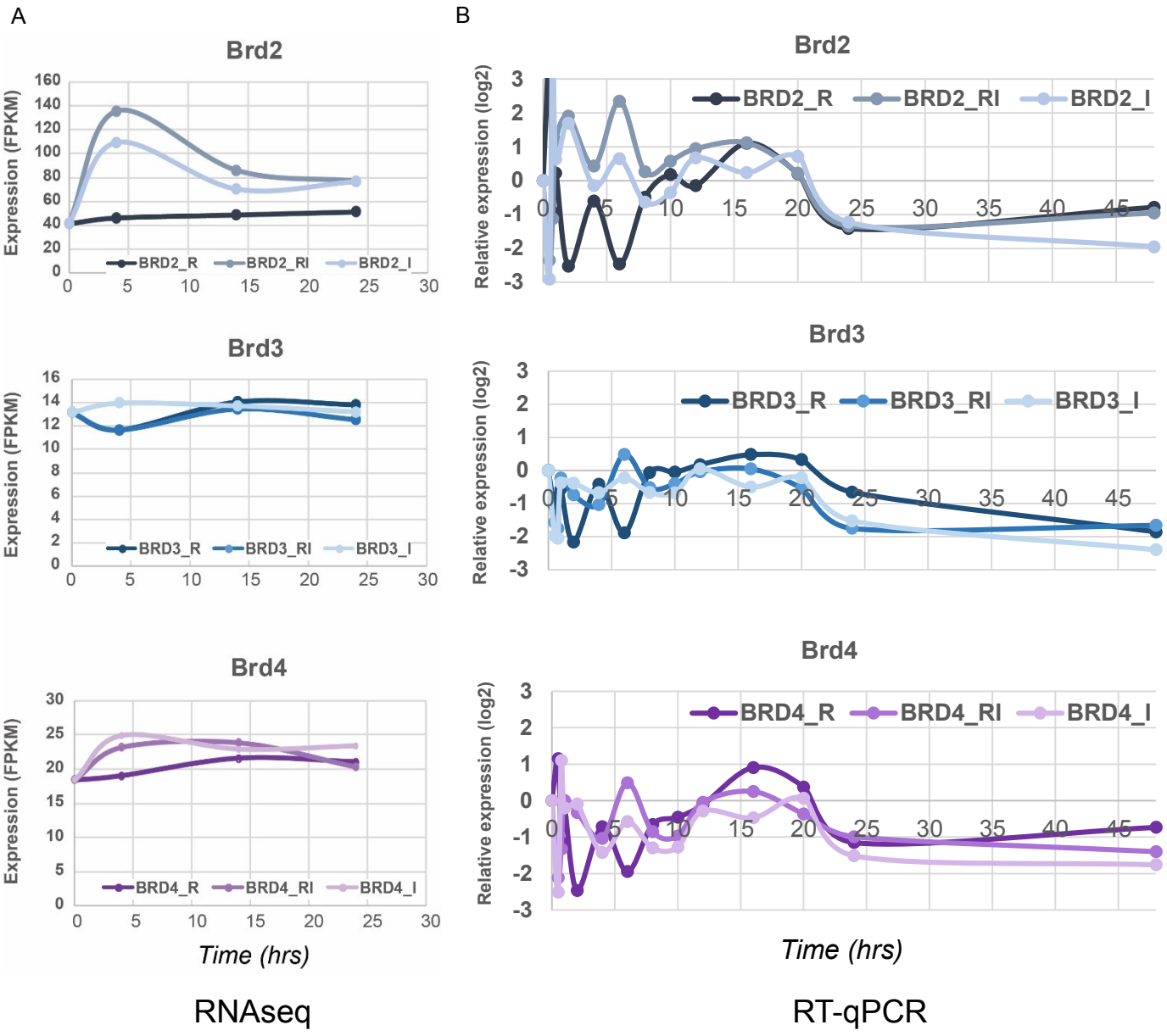

Suppl Figure 3

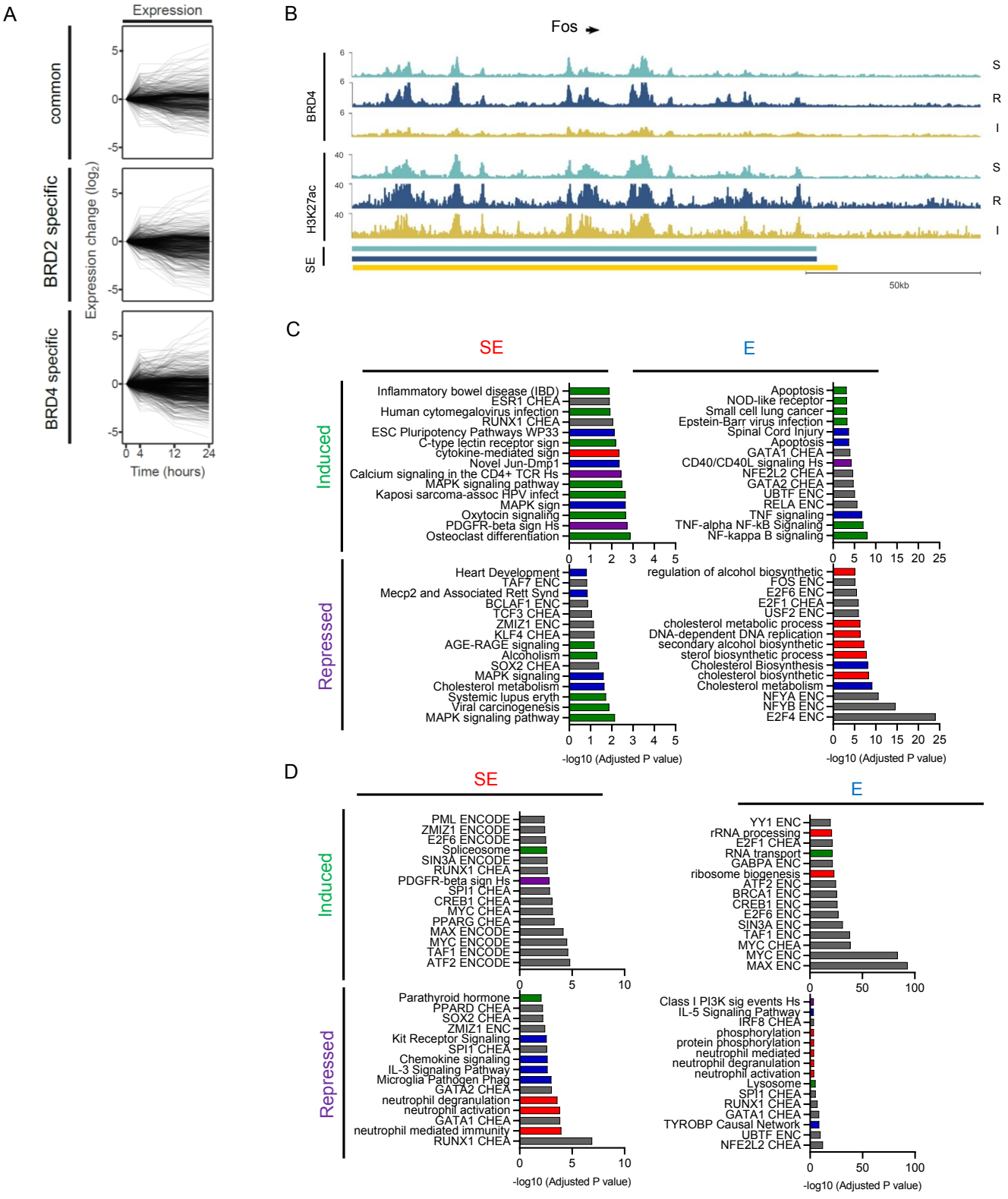

Suppl Figure 4

A

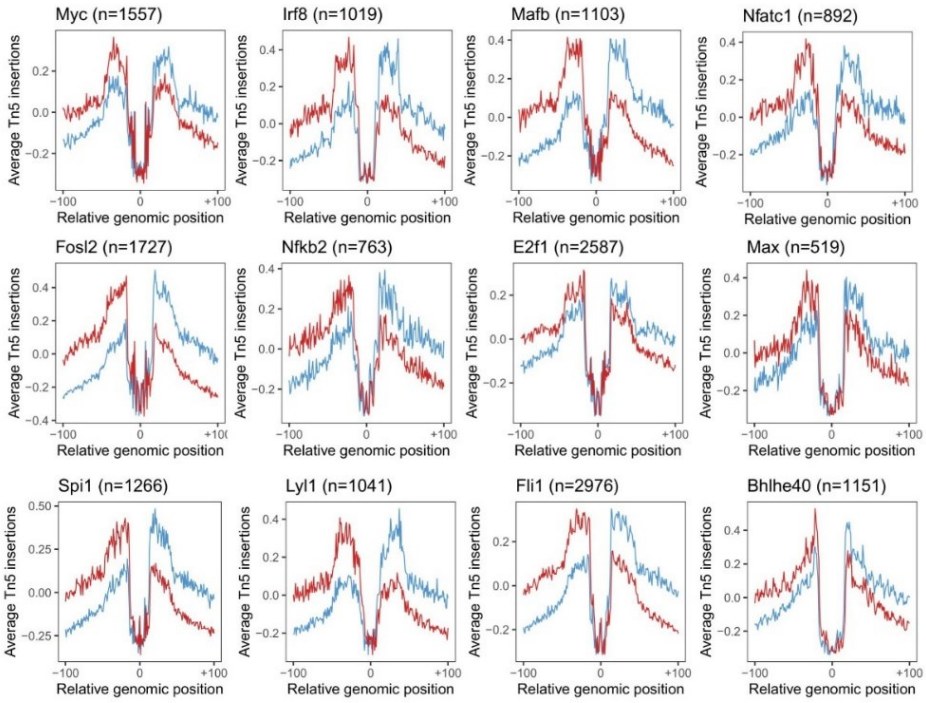

B

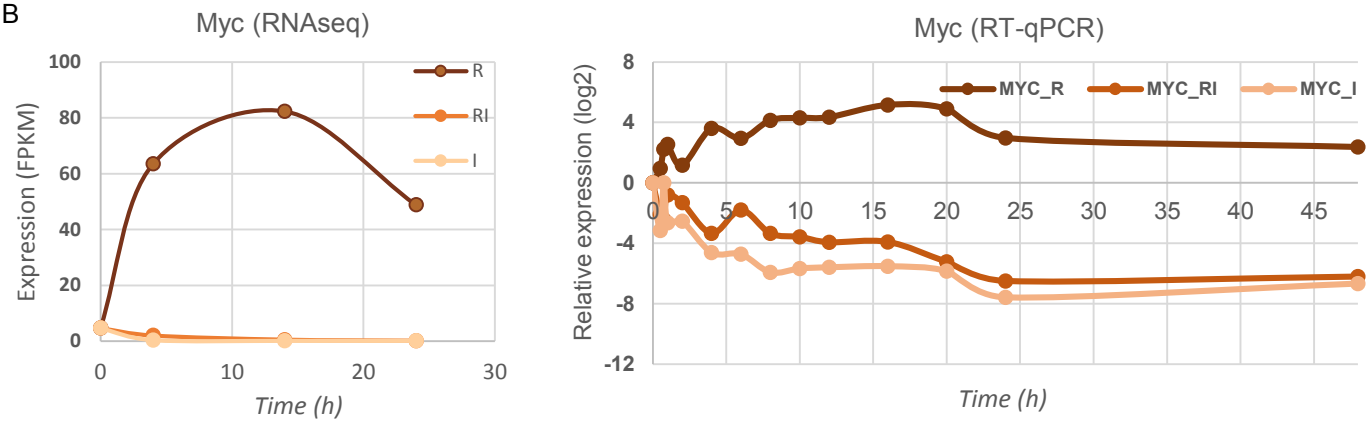

C

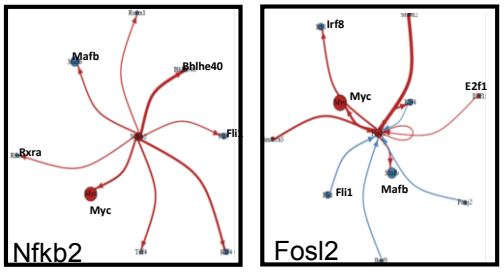

Suppl Figure 5

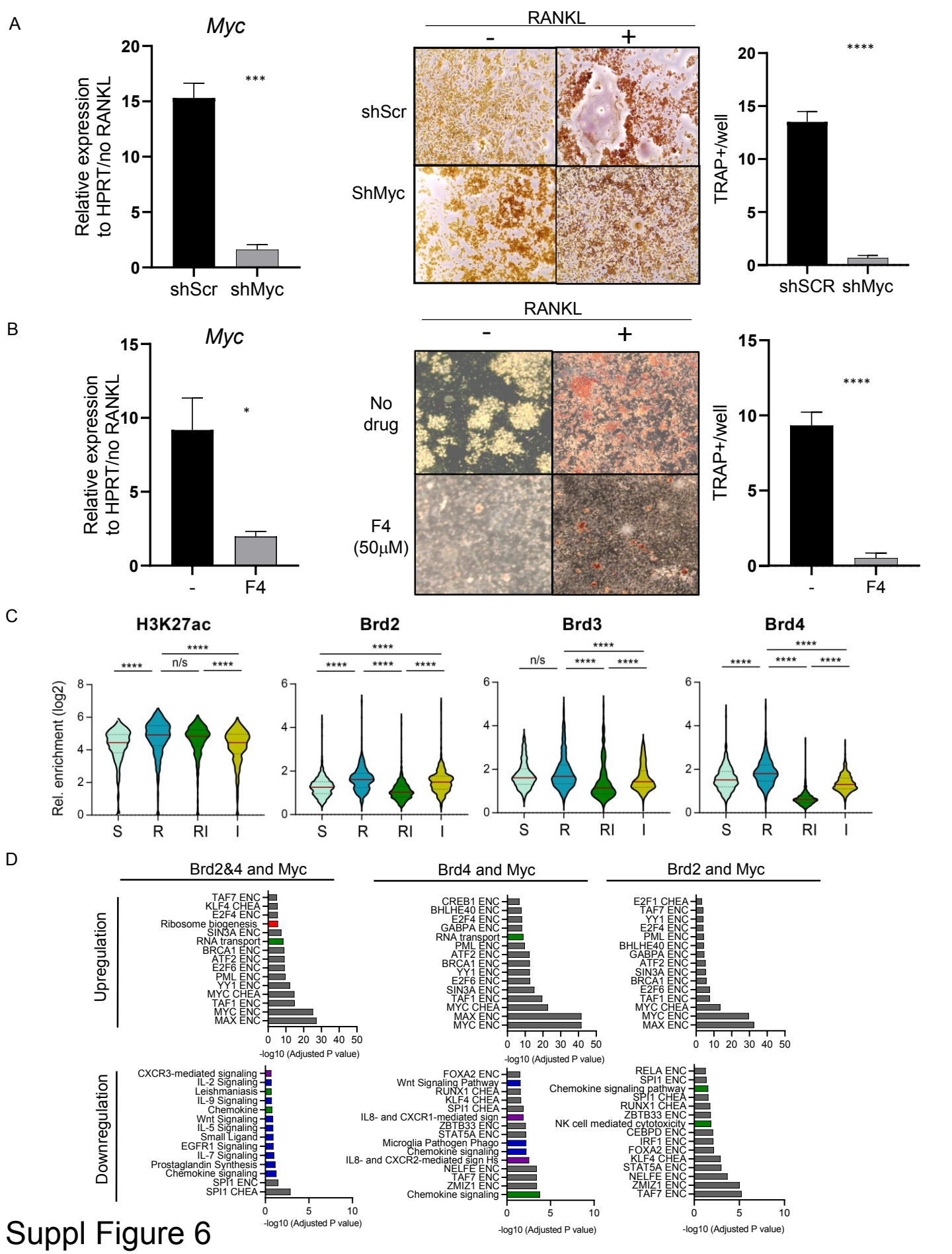

Suppl Figure 6